LAWRENCE
LIVERMORE
NATIONAL
LABORATORY

LLNL-TR-661898

Results of the NEL Shot-Rate Campaign

S. Sutton, C. Marshall, C. Hayman

Septemer 29, 2014

This document was prepared as an account of work sponsored by an agency of the United States government. Neither the United States government nor Lawrence Livermore National Security, LLC, nor any of their employees makes any warranty, expressed or implied, or assumes any legal liability or responsibility for the accuracy, completeness, or usefulness of any information, apparatus, product, or process disclosed, or represents that its use would not infringe privately owned rights. Reference herein to any specific commercial product, process, or service by trade name, trademark, manufacturer, or otherwise does not necessarily constitute or imply its endorsement, recommendation, or favoring by the United States government or Lawrence Livermore National Security, LLC. The views and opinions of authors expressed herein do not necessarily state or reflect those of the United States government or Lawrence Livermore National Security, LLC, and shall not be used for advertising or product endorsement purposes.

This work performed under the auspices of the U.S. Department of Energy by Lawrence Livermore National Laboratory under Contract DE-AC52-07NA27344.

Interdepartmental Memorandum

Mail Station L-463

Ext: 2-0322

January 12, 2004
NIF-0110452-AA

TO: Distribution

FROM: Steve Sutton, Chris Marshall and Chris Haynam

SUBJECT: **Results of the NEL Shot-Rate Campaign**

Executive Summary

Experiments to quantify the thermally induced optical distortions associated with shot rate have been successfully designed and conducted. In these test, sets of shots at 4-hour, 2.5-hour, and 1.5-hour shot periods were performed. Measurements of wavefront distortion were made using the OSP Hartmann sensor, the PDS Hartmann sensor, and the PDS Far-field camera. These tests demonstrated that around the clock operation with 4-hour shot period and no significant focal spot degradation is feasible. Additionally, "burst" mode operation at shot periods as short as 1.5 hours appears possible, with minimal increase in focal spot size. These tests successfully showed that the NIF cooling system performed as expected, and that the cooling approach is technically sound.

1. Introduction

In November 2003, a shot campaign designed to quantify the effect of shot-rate on beam quality was conducted. This campaign consisted of sequences of flashlamp firings at 4-hour, 2.5-hour, and 1.5-hour intervals, on an 11-3 configuration at a 20% explosion fraction. During the tests, extensive wavefront data was collected using the OPS (Hartmann sensor) and PDS (Hartmann sensor, Far-field) diagnostic packages.

It is useful to review the origins of shot-rate issues, and the motiviation for the cooling approach employed in NIF. Efforts to enhance shot rate through active cooling of heated elements in the laser chain date back to NOVA, where the focus was on gas flow through the slab cavity. This approach proved to be troublesome, and was abandoned [1].

No effort was made to cool the Beamlet laser, which was a NIF physics testbed. Data from that laser, however, did demonstrate the need for active cooling of the amplifiers. Fig. 1 gives two far-field images associated with the first and third shots of a day (data taken on 8/30/96), where the shots were separated by an average of ~2 hours [1]. Note that the 80% enclosed energy radius increased by nearly a factor of two by the third shot (after the heating of two shots), and the brightness was reduced by over a factor of three. It was primarily these observations on Beamlet that motivated the implementation of active cooling on NIF. The NIF cooling approach was demonstrated in AMPLAB tests [2]. While efforts to measure optical distortions were unsuccessful, slab, blastshield, and flashlamp temperatures were measured which showed thermal recovery. The measurement temperatures were successfully compared to model calculations.

The present memo summarizes the data taken during the recent shot-rate tests. There were over 2000 Hartmann sensor images (OSP and PDS) collected during the course of these tests, as well as nearly 100 1w far-field images. One of the primary purposes of this campaign was to provide data for validation of the numerical models that have been used to predict NIF optical performance. This comparison is on-going, and will be reported in detail in a subsequent memorandum.

2. Shot-Rate Campaign Overview

The shot-rate campaign is summarized in Table 1. Three shot series were conducted at periods of 4 hours, 2.5 hours, and 1.5 hours. During each series, efforts were made to keep the aerosol purge time and flashlamp cooling time consistently the same. While 30 minutes of aerosol purge was performed following each shot, the flashlamp cooling time did vary between shot sets. During this campaign, there was no injection during the flashlamp firing in order to expedite the test sequence and allow consistent spacing between flashlamp firings. All wavefront distortion data was collected prior to the flashlamp firing, and thus represents the residual thermal distortions that would be present at shot-time.

The shot time-line is given in Fig. 2, which identifies the timing of important events that took place between shots. While there was no injection during the flashlamp firing, efforts were made to conduct the test in a manner consistent with the projected operating mode of NIF. For example, it is anticipated that final alignment and shot preparation will take no less than 1 hour. So, flashlamp cooling was turned off no less than 1 hour prior to the next shot. Additionally, 30 minutes of aerosol purge was performed consistent with current and projected NIF requirements. Note that as a result of these time constraints, data collection took place as much as 60 minutes prior to the next shot. Thus, while the data

collected accurately quantifes the thermal distortion at data collection time, this data set does not quantify any changes that might have taken place in the time between the conclusion of data collection and the next shot.

Data collected using the OSP Hartmann sensor, employing the ISP beam, consisted of two sets: (1) a set of roughly 40 images, spaced 5 seconds apart, where the deformable mirror (DM) was returned to the "first-of-the-day" flat wavefront configuration, and (2) a set of roughly 40 images, spaced 1 second apart, where the first ten were under closed-loop, flat wavefront mode, and the remainder were with the mirror frozen (open-loop). This last set was designed to address "T-1" considerations. Both sets were collected prior to each flashlamp firing.

In addition to the OSP data, PDS Hartmann sensor and PDS 1w far-field camera data were collected. Prior to each flashlamp firing, 40 PDS Hartmann sensor images were collected using the Regen beam. These images were spaced at roughly 5 second intervals, with the DM frozen in a flat wavefront state (open-loop after closed-loop flat wavefront). Additionally, from three to six 1w far-field images were also collected using the Regen beam. The far-field images were collected over a 2 to 3 minute period, again with the DM in a frozen flat wavefront state.

3. Data Summary

Data discussed in this section is organized according to the diagnostic package used and the purpose of the collected data.

Temperature Data

There is active logging of a number of sensors in the flashlamp cooling system, including outlet gas temperature in the bundle header. This outlet gas temperature for the three shot sets is given in Fig. 3. Each flashlamp firing and subsequent "turning on" of the cooling system is indicated by the abrupt increase in temperature. The inflection points in the decay following a flashlamp firing indicates the time when the cooling system was turned off. These inflection points are identified in the plots on the first and last shots of each set. The data following this inflection point (up until the next shot) is not representative of temperature conditions inside the amplifiers since the cooling flow was off. Note that the cooling gas discharge temperature is unchanged for the 4-hour shot period set, indicating that 2.5 hours of flashlamp cooling is adequate to remove all waste heat from the flashlamps. On the other hand, the 2°F temperature rise during the six shots in the 1.5 hour set clearly indicates that ½ hour of flashlamp cooling is not adequate to

remove the waste heat from the flashlamps. As will be subsequently shown, this will be reflected in the measured optical distortions.

PDS Far-Field Data

Data collected using the PDS far-field camera is summarized in Fig. 4, which gives the 1w 80% enclosed energy radius as a function of shot number for the three shot sets. Also indicted on this figure is the NIF requirement that residual thermal distortions from prior shots add no more than 2.5 microradians to the beam divergence, as compared to the cold system [3]. In this instance, this limit is shown with respect to the average of the cold system (shot 1) values. There are several important observations:

a. There is clearly a negligible change in the 4-hour data. In fact, the far-field radius decreases with shot number, which is likely an indication of the experimental uncertainty associated with this measurement since there is no rational reason to expect the system performance to get better at elevated temperature.
b. In the images collected for any given shot, there is as much as a $\pm 7\%$ variation. This is most likely due to convection driven gas distortions (turbulence) in the amplifier cavities, but could also contain unquantified vibration effects.
c. With few exceptions, the NIF requirement is achieved on all shots for the three shot rates considered.

In addition, efforts were made to use the PDS far-field data to quantify the effect of residual thermal distortions on beam pointing. The variation of the PDS far-field centroid with data sample is given in Fig. 5 for two sets. This data is from the 1.5 hour shot period tests, with one sequence for the cold system (first of the day data set), and the other for the 5th shot (4 flashlamp firings). There is not obvious trend, with the scatter likely due to PDS vibration problems.

OSP Hartmann Sensor "T-1" Data

One of the OSP Hartmann sensor data sets was designed to address the need for a "T-1" system on NIF. This was motivated by Beamlet data that showed a significant degradation in the wavefront in the first few seconds after going open loop, for both cold and heated amplifier states [4]. During the shot-rate tests, this data was collected prior to each shot, and consisted of 40 OSP Hartmann sensor images spaced 1 second apart. The first ~10 seconds of data was collected with the DM in closed-loop, flat wavefront configuration. The mirror was then frozen (open-loop), and data collection continued for

an additional ~30 seconds. Thus, we are able to see the distortion changes that take place after going open-loop. An analysis extension was to turn the measured wavefront into a predicted far-field. This was accomplished using an algorithm provided by Wade Williams that used a generic intensity profile. Reconstructed wavefront and far-field values for the three shot sets are given in Figs. 6 through 8.

First consider Fig. 6 which is for the 4-hour shot period set. Fig. 6a gives the reconstructed wavefront peak-to-valley (P-V) for the first set (prior to shot #1) and the final set (prior to what would have been shot #5). Corresponding plots for the wavefront RMS gradient (Fig. 6b), calculated 1w 80% enclosed energy radius (Fig. 6c), and the beam pointing change (Fig. 6d). The gray bar in each plot roughly denotes the time when the mirror went open loop. There is uncertainty in the actual time that this change took place since this was a manual timing operation. Beam pointing was determined by averaging the Hartmann sensor focal spot offsets, and adjusting the calculated pointing change by the 1st data point value. This was necessary since there was a systematic offset between data sets due to alignment considerations. In these plots we see little evidence of change after going open loop.

Corresponding plots for the 2.5 hour shot period set are given in Fig. 7. In this case we do see substantial changes (>20% in P-V, >15% in far-field radius) in the wavefront within 5 seconds after going open loop. This data clearly shows the benefit that a “T-1” system would have if uncertainties of this magnitude are unacceptable. Note that when comparing the cold system and 7th shot data, there is a substantial closed loop offset in both the far-field radius and the wavefront RMS gradient, which shows the first signs of DM correction difficulties.

The final set of plots for the 1.5 hour set are given in Fig. 8. These also show substantial changes (>35% in P-V, >30% in far-field radius) in the wavefront in the first 5 seconds after going open loop. In this set it is important to note the wide variation in the closed loop data for the 7th shot set. This indicates that the deformable mirror is unable to completely correct the residual distortions either because the scale sizes are too small, the frequency is too high, or because the mirror response has not been adequately tuned. Unfortunately, the present data sets do not allow differentiation of these contributions.

One additional feature to note in Figs. 7 and 8 is the periodic structure in the P-V, RMS gradient, and half-angle plots. There is structure in these plots that has a roughly 10 second period. This most likely corresponds to low frequency convection instabilities that have been previously identified [5].

Following collection of the 7th shot data set in the 1.5 hour series, an extended “T-1” data set was collected. In this case, images were stored every 20 seconds. There was

~5 minutes of closed-loop operation followed by ~30 minutes of open-loop data collection. The wavefront properties extracted from this data set are given in Fig. 9. In this instance, we see much larger scatter in the data after going open-loop than was evidenced in the shorter time window set reported in Fig. 8. However, the maximum change in the far-field radius is still ~30%. The anomalous behavior in the beam pointing plot (Fig. 9d) was due to a pressure reduction in the main amplifier cavity, which took about 10 minutes to fully recover. Some effect of this reduction can be seen in the other plots, but not as significantly as shown in Fig. 9d. Since the system pressure is increased while the cooling system is operating, this clearly indicates one reason that alignment must wait until the cooling system is turned off.

Fig. 10 gives the overall variation in the reconstructed wavefront P-V over the last 20 images in each "1 second" set. Note that this covers a time from roughly 10 seconds after going open loop until about 30 seconds after going open loop. There is clear evidence of the heating effect in the 2.5 hour and 1.5 hour sets, as the variance is increasing with increased system temperature (or increased shot number). The anonymously high 1.5 hour shot 6 value cannot be explained at this time.

Fig. 11 gives the change in the P-V that takes place when going open loop. This is the difference between the average of the last 20 images in the 40 image set (open-loop values) and the average of the first 8 images in the set (closed-loop values). The effect of heating is clearly shown in this data set, but the scatter is also striking.

PDS Hartmann Sensor Data

Prior to each flashlamp firing, at least 40 PDS Hartmann sensor images were collected with the DM open-loop, following closed-loop flat wavefront correction. This data was analyzed as follows:

a. The wavefront was reconstructed for each of the images collected, employing a consistent rectangular mask to eliminate edge variations. The zonal reconstruction method was employed in the Wavefront Sciences software.
b. The reconstructed wavefront set was then averaged to establish a static distortion baseline.
c. The static distortion baseline was then subtracted from each wavefront in the set in order to extract the dynamic component.

The purpose of this data analysis approach was to extract the thermally driven gas distortions, which are associated with heating in the amplifiers. By subtracting the static distortion baseline, which is a combination of true static distortions, mirror residual errors

(which are constant since the mirror was frozen while the data was being taken), and very slowly varying thermal distortions, we are left with the time varying component which is associated with the unstable convective flowfield. The results of this analysis are given in Figs. 12. Fig. 12a gives for each shot the average P-V of the 40 data points collected. There is clear evidence of heating effects in the 2.5-hour and 1.5-hour sets. For each data set, the overall variation in the wavefront P-V is given in Fig. 12b. In general the increased variation with shot number is consistent with expected heating effects, but the trends are less striking than in Fig. 12a. Finally, the average wavefront RMS gradient (average of the 40 data values in each set) is plotted in Fig. 12c. This again shows a shot-rate effect and is consistent with Fig. 12a. The RMS gradient values are in arbitrary units since there is still some uncertainty in the scaling of the lenslet spacing on the Hartmann sensor to the NIF full beam size.

OSP Hartmann Sensor Slab Distortion Data

The final set of data to be discussed is associated with the thermally driven distortions in the laser slabs. This data was obtained using the OSP Hartmann sensor, and collected and analyzed as follows:

a. Prior to each shot, the DM was place in the reference flat position.
b. 40 images were then collected, spaced approximately 5 seconds apart.
c. The reconstructed wavefronts for the 40 Hartmann sensor images were then averaged in order to reduce the magnitude of any incoherent contributions and isolate the static distortions and slowly varying coherent distortion components.
d. The cold system (shot #1) averaged wavefront was then subtracted from the subsequent shot averages. This is intended to isolate the slab thermal distortions.

The P-V of this extracted distortion is presented in Fig. 13 for the three shot sets. The spatial distribution of the distortion is shown in Figs. 14 through 16. Referring to Fig. 13, until shot #6 of the 2.5-hour and 1.5-hour sets there is a clear increasing trend with shot number. The sudden drop with shot #6 is most likely due to an inadvertent change in the mirror state, i.e., the reference flat was most likely altered. Unfortunately, the ICCS action logs do not provide adequate information to ascertain if this actually happened.

Looking at Figs. 14, there is no clear consistent structure in the 4-hour shot period set. This likely indicates that the slowly changing slab distortions in this sequence are varying within the measurement noise. Another explanation is that new reference flat files were taken each time. Once again, this can't be verified.

Moving on to the 2.5-hour (Fig. 15) and the 1.5-hour (Fig. 16) sets, there is clearly consistent structure through the 5th shot. Once again, the change with the 6th shot in both cases is most likely due to an inadvertent change in the mirror state. Also note that there is a significant shape difference between the 2.5-hour and 1.5-hour sets. The wavefront shape in the 2.5-hour set (Fig. 15) is generally consistent with model predictions. An example of the predicted wavefront from detailed numerical simulations is given in Fig. 17, for 3 hours after a single shot [6]. This shows the same basic structure, with the experimental measurements being significantly less symmetric than the model predictions. This saddle shape is indicative of optical distortions governed by warping of the slab (the so-called "potato chip" warping). The striking shape difference between the 2.5-hour and 1.5-hour sets will be studied as part of ongoing analysis efforts to be reported in a subsequent memorandum. However, the distortion shape in Fig. 16 is more indicative of optical distortions driven directly by temperature contributions to the index of refraction, in this case most likely from edge effects due to the hotter edge cladding present at this shot rate.

4. Summary and Conclusions

As a result of this sequence of shot-rate measurements, some fundamental conclusions can drawn:

1. *The demonstrated wavefront recovery rate meets NIF requirements*. These results demonstrated the viability of around the clock operation with 4-hour shot period and no significant degradation in focal spot size. They also indicate that "burst" mode operation at shot periods as short as 1.5 hours is feasible, with minimal increase in spot size.
2. *The flashlamp cooling system worked as designed*. This is a significant accomplishment, noting that active cooling of the NOVA laser was abandoned after initial tests proved unacceptable.
3. *A "T-1" system does not appear to be necessary*. The "T-1" data indicates that at long shot periods (say 4-hours or more), a "T – 30 second" system is adequate. For the higher shot rate cases, as much as a 20% improvement in focal spot could be achieve using a "T-1" system.

In addition, there are a number of open issues that should be addressed as part of ongoing analysis and experiment efforts. These include:

1. *Quantification of any shot rate limits due to the edge cladding bonding epoxy temperature limit*. The edge cladding epoxy limit is 93°F (34°C). Both calculations and temperature measurements indicate that this limit could be an

issue with extended operation at 2.5-hour and 1.5-hour shot periods. There does not appear to be any issues at a 4-hour shot period.

2. *Quantification of DM drive voltage limits*. The DM actuators have a ±10 volt drive limit. With the 11-7, 18% pre-shot figure used in these studies, the maximum voltage observed was 5.5 volts. With higher explosion fractions or a fewer number of power amplifier slabs this will increase.
3. *Comparison of model predictions to measurement*. Evaluation of the models under high shot-rate conditions is ongoing. Part of this effort will be to correct any heat transport deficiencies, and recalibrate the temperature-to-wavefront correlations.
4. *Measurement of the 3w far-field*. It is important that "true" shot-rate tests (shots with injection) to PDS be scheduled in order to quantify the 3w far-field. These would represent the ultimate shot-rate verification experiments.

Acknowledgements

These tests required the cooperation of far too many NIF personnel than can be appropriately mentioned. In particular, the efforts of the beam control, industrial control, and PDS operators, and the NIF shot directors, are acknowledged and appreciated. Additionally, appreciation is extended to Wade Williams for providing the algorithm for generating the far-field.

References

1. K. Manes, private communication, November 2003.
2. A. Erlandson (Ed.), "Physics Basis for Optical Performance of the NIF Amplifiers," NIF-0014142, January 11, 1999.
3. This is taken from NIF requirement 5500007.
4. R. Hartley, et. al., "Wavefront correction for static and dynamic aberrations to within 1 second of the system shot in the NIF Beamlet demonstration facility," SPIE, Vol. 3047, p. 294.
5. S. Sutton, "An update on NIF gas distortion characterization – Scaling and focal spot size effects," NIF-0082390-0B, May 23, 2002.
6. Based on simulation results provided by Wayne Miller.

Table 1
Shot-rate campaign summary

Date	Shot period (hours)	Number of shots	Flashlamp cooling time	Aersol purge time
11/19/03	4	4	~2.3 hours	30 minutes
11/20/03	2.5	6	~50 minuts	30 minutes
11/24/03	~1.5*	6	~30 minutes	30 minutes

* Shot period varied from 1.6 to 1.9 hours

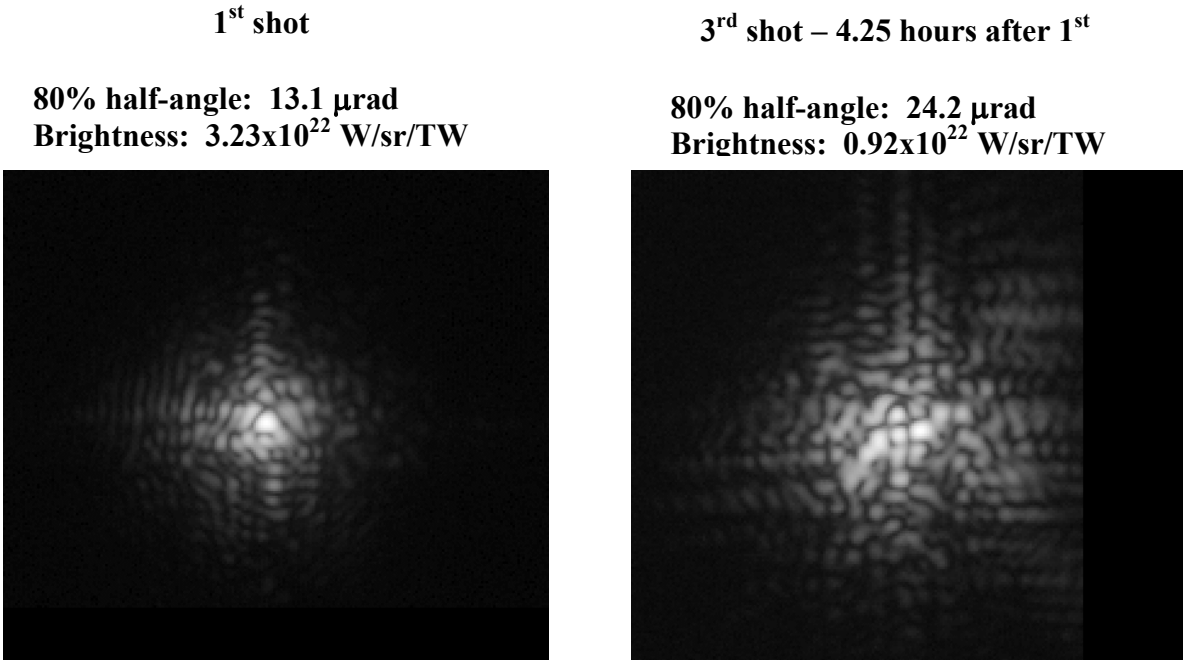

Fig. 1 - Images of the Beamlet 1w far-field taken on three shots spaced 4.25 hours apart, which is roughly representative of a 2 hour shot period. Note that there is nearly a doubling of the focal spot radius due to the heating from two shots. This data was taken on 8/30/96.

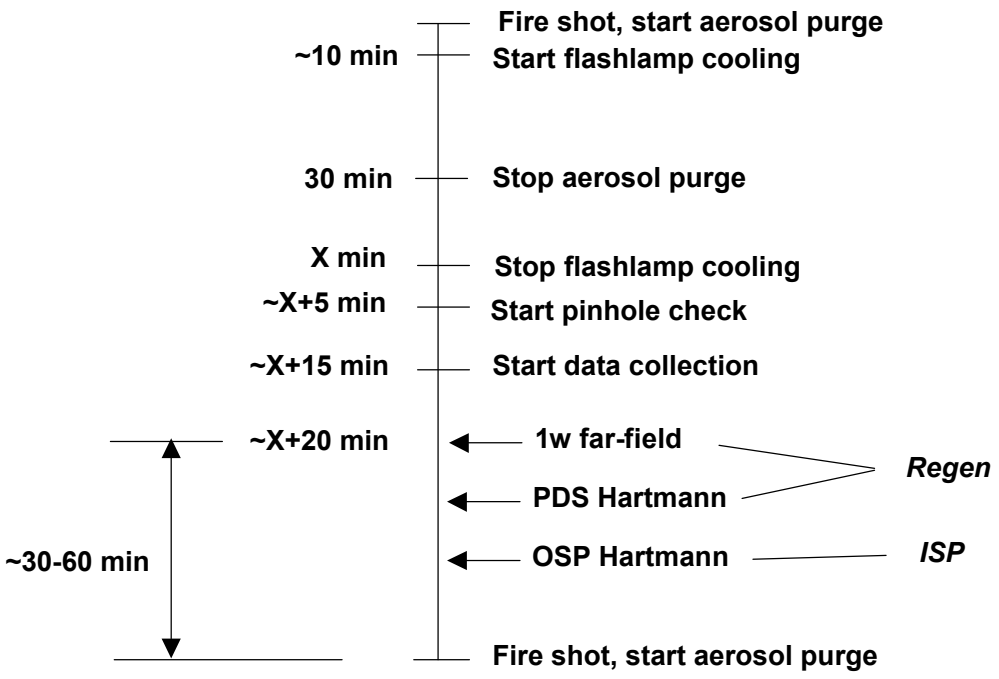

Fig. 2 - The time-line of events between shots. Note that data was collected prior to the first shot, and following the last shot (prior to what would have been a next shot).;

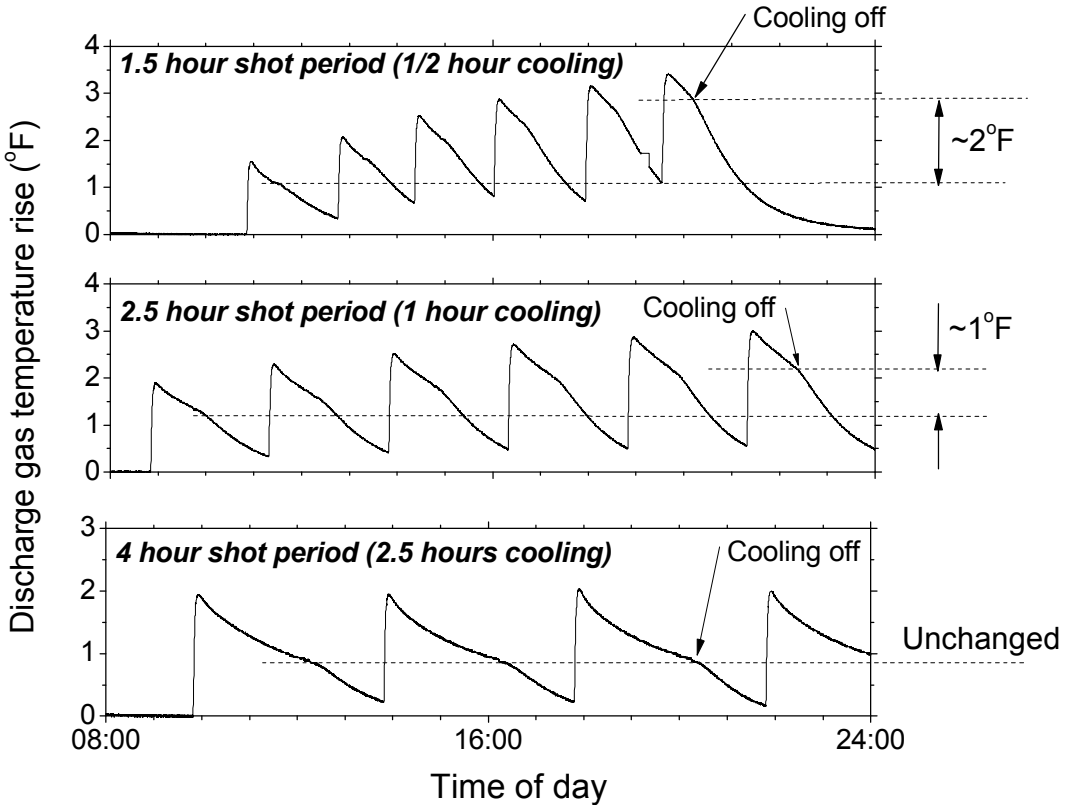

Fig. 3 - The flashlamp cooling loop discharge temperature as measured at the bundle header. The inflection points in the decay portion of the traces indicates the point where the cooling system was turned off.

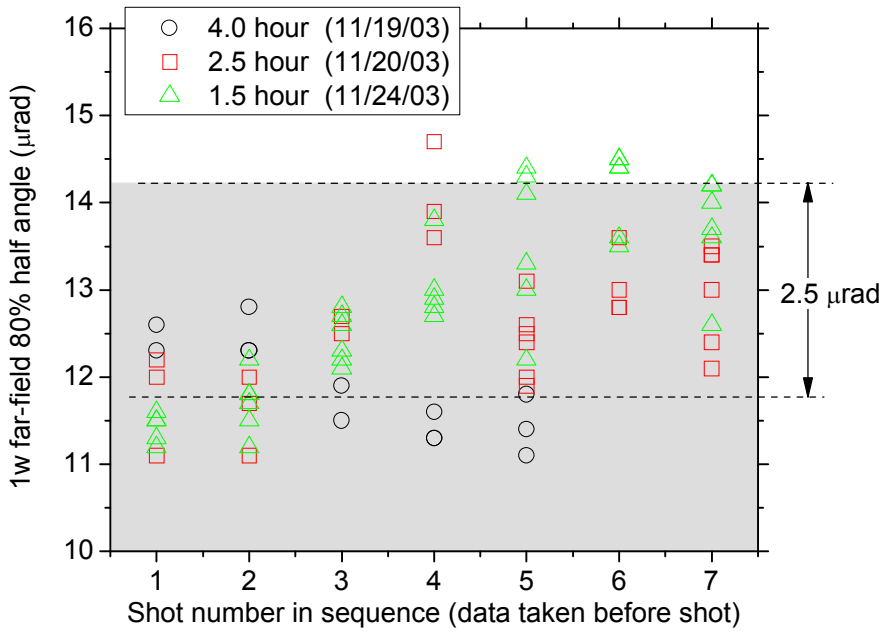

Fig. 4 - The measured far-field radius as a function of shot number in each of the three shot sets. The gray region represents the acceptable domain as given by the NIF requirement that residual thermal distortions add no more than 2.5 microradians to the beam divergence.

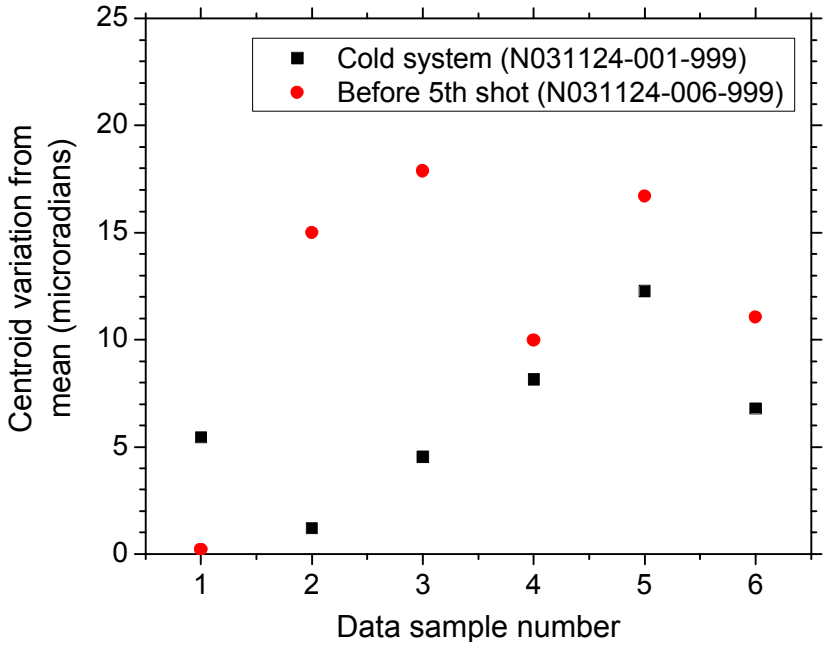

Fig. 5 - The measured far-field centroid location variation during two data collection sequences. This data is inconclusive, but does demonstrate vibration problems inherent in the PDS system.

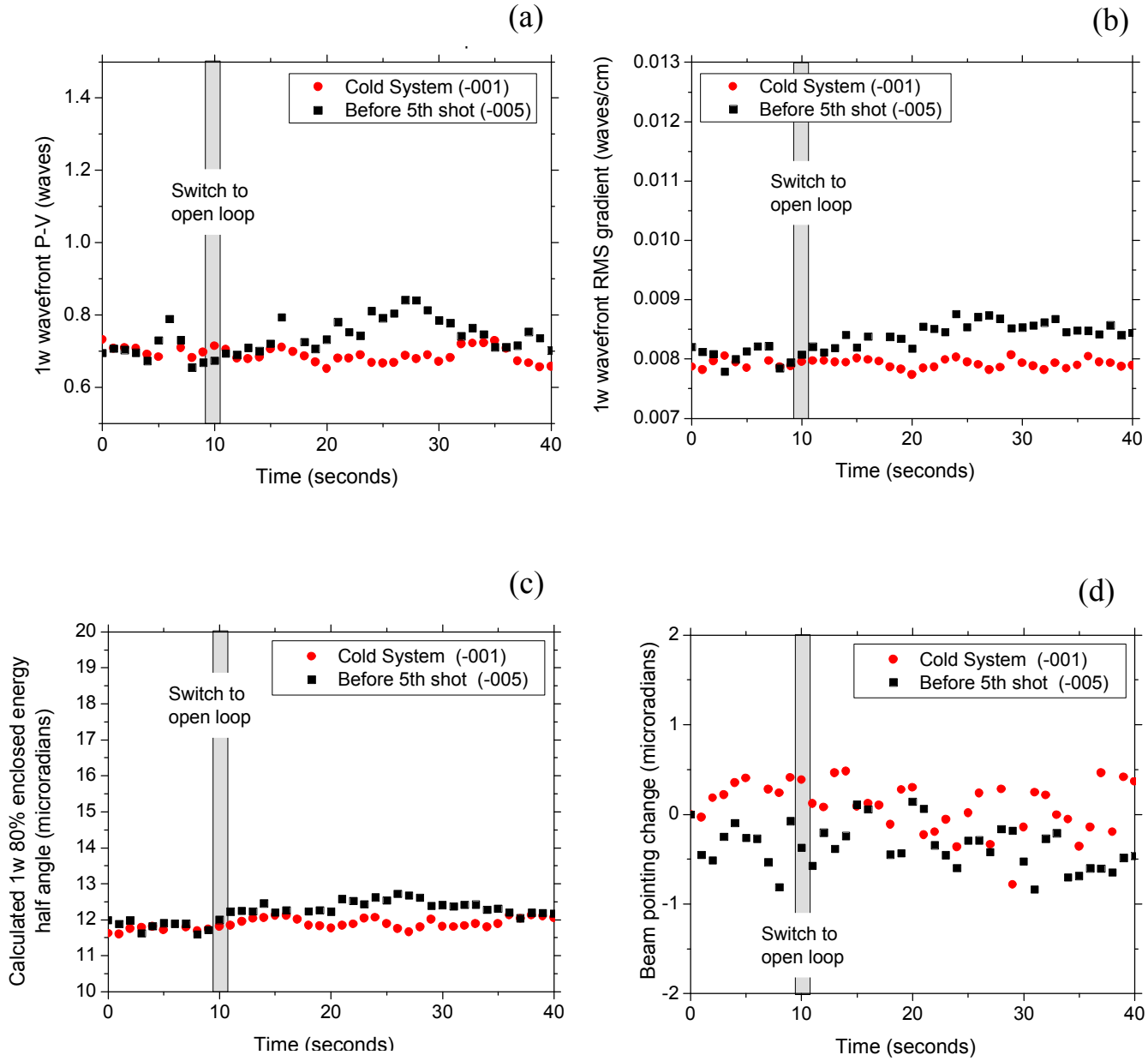

Fig. 6 - Reconstructed "T-1" wavefront data for the 4-hour shot period set. (a) Wavefront peak-to-valley. (b) Wavefront RMS gradient. (c) Calculated far-field radius. (d) Beam pointing changes.

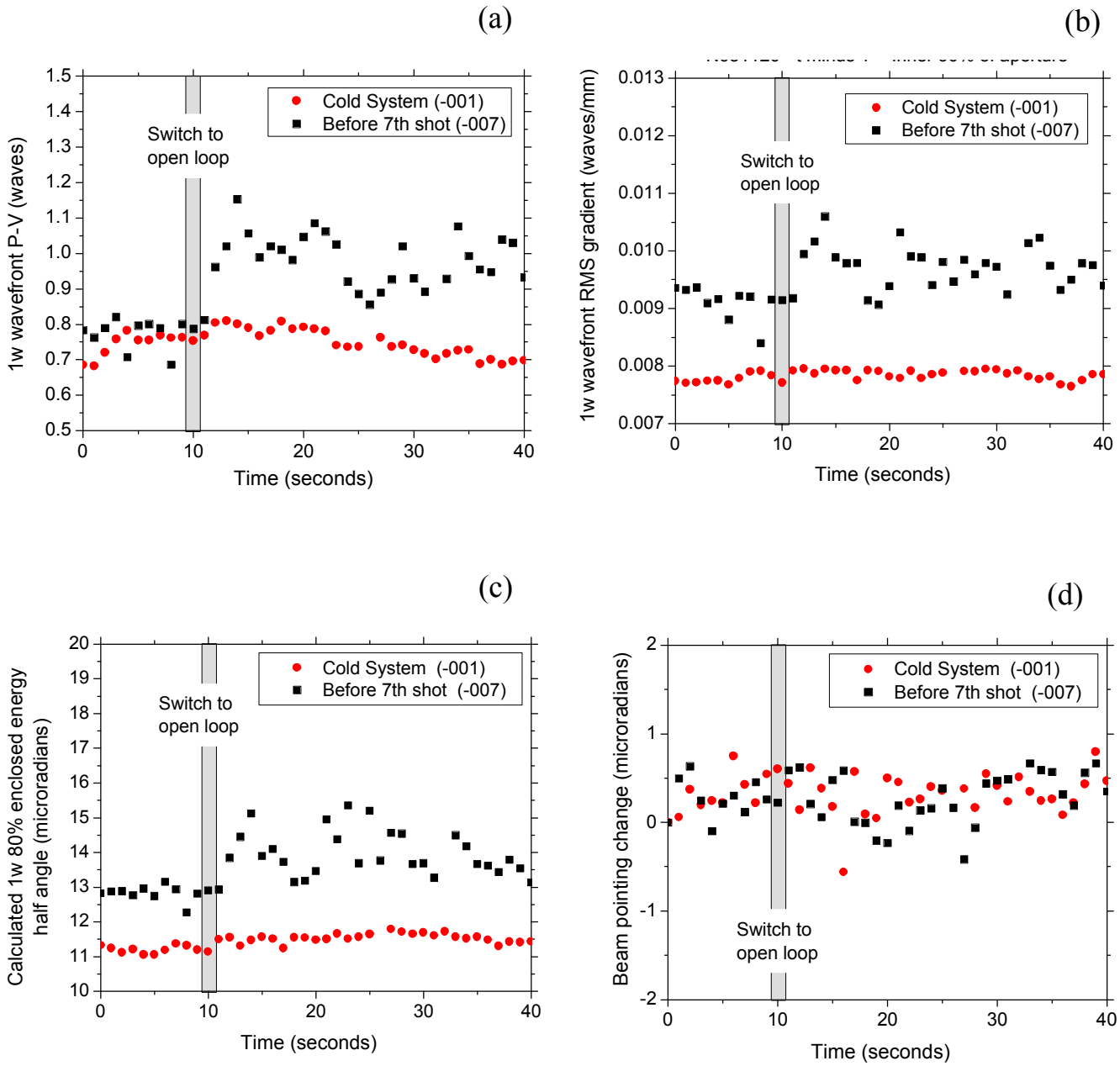

Fig. 7 - Reconstructed "T-1" wavefront data for the 2.5-hour shot period set. (a) Wavefront peak-to-valley. (b) Wavefront RMS gradient. (c) Calculated far-field radius. (d) Beam pointing changes.

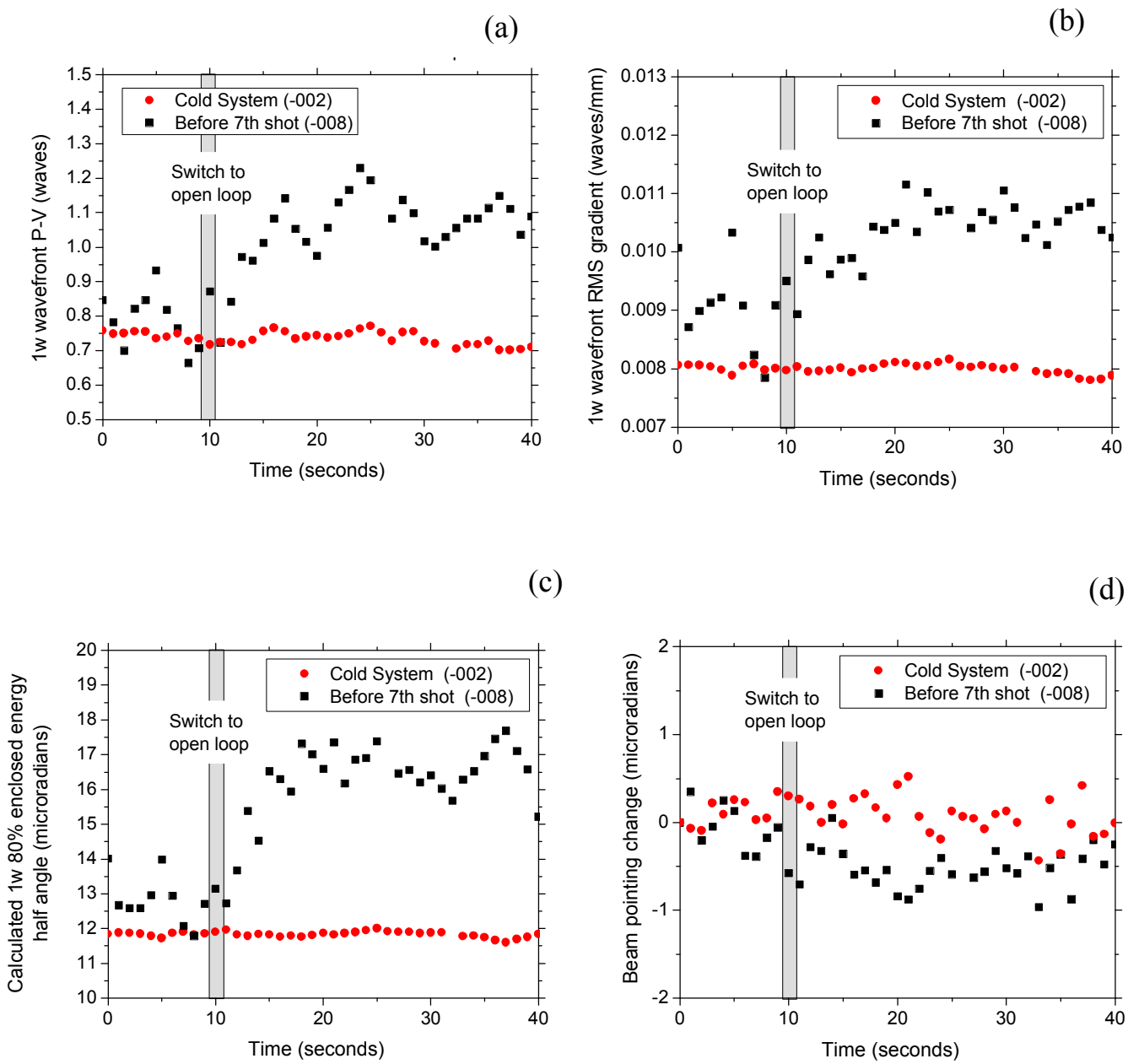

Fig. 8 - Reconstructed "T-1" wavefront data for the 1.5-hour shot period set. (a) Wavefront peak-to-valley. (b) Wavefront RMS gradient. (c) Calculated far-field radius. (d) Beam pointing changes.

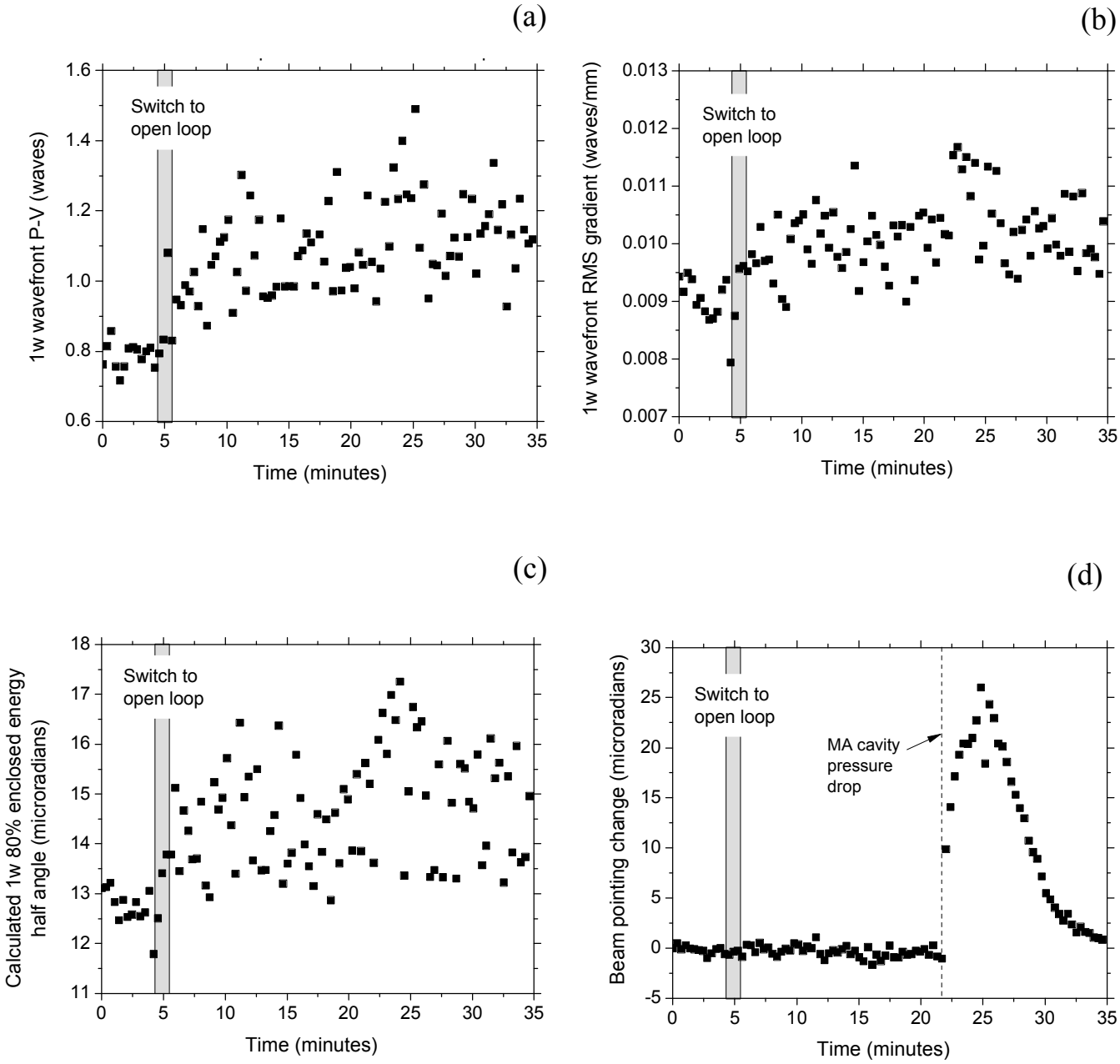

Fig. 9 - Reconstructed extended "T-1" wavefront data for the 4-hour shot period set. (a) Wavefront peak-to-valley. (b) Wavefront RMS gradient. (c) Calculated far-field radius. (d) Beam pointing changes.

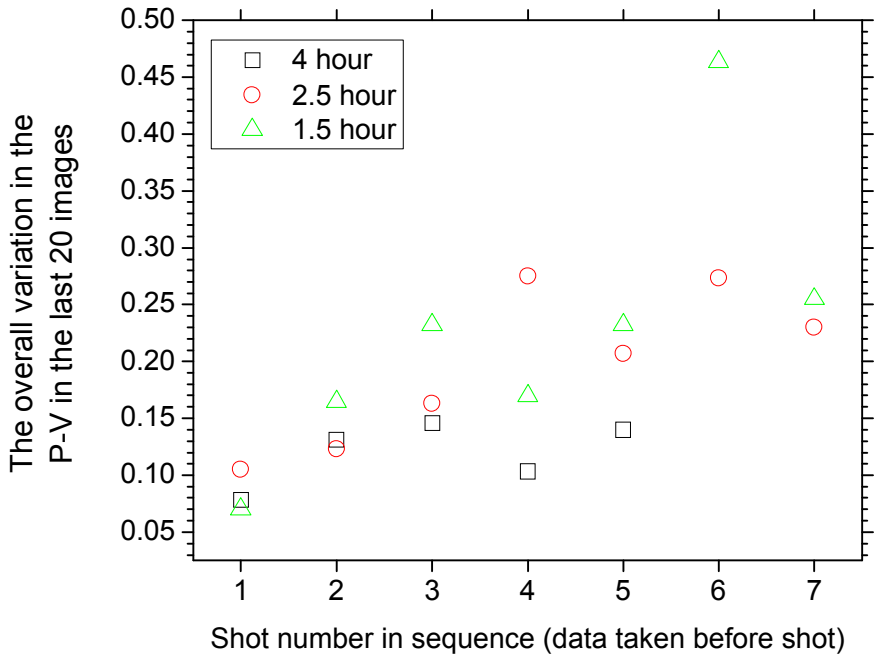

Fig. 10 - The overall variation in P-V of the reconstructed wavefront of the last 20 images of each data set. Note that this is the average of data taken from 10 to 30 seconds after going open loop.

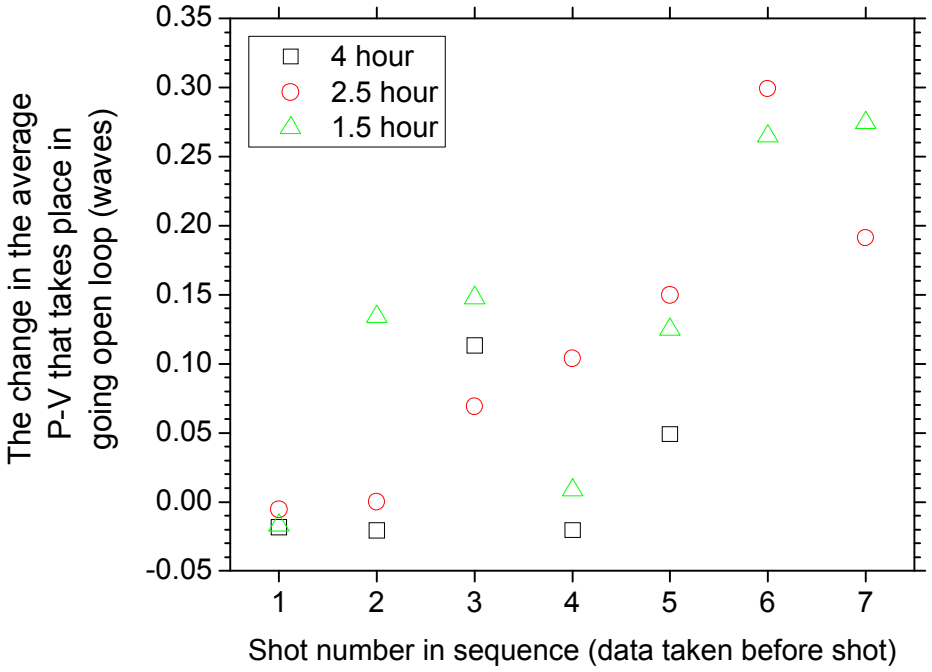

Fig. 11 - The change in the average P-V that takes place in going open loop. This is the difference between the average P-V of the first 8 images and the average P-V of the last 20 images.

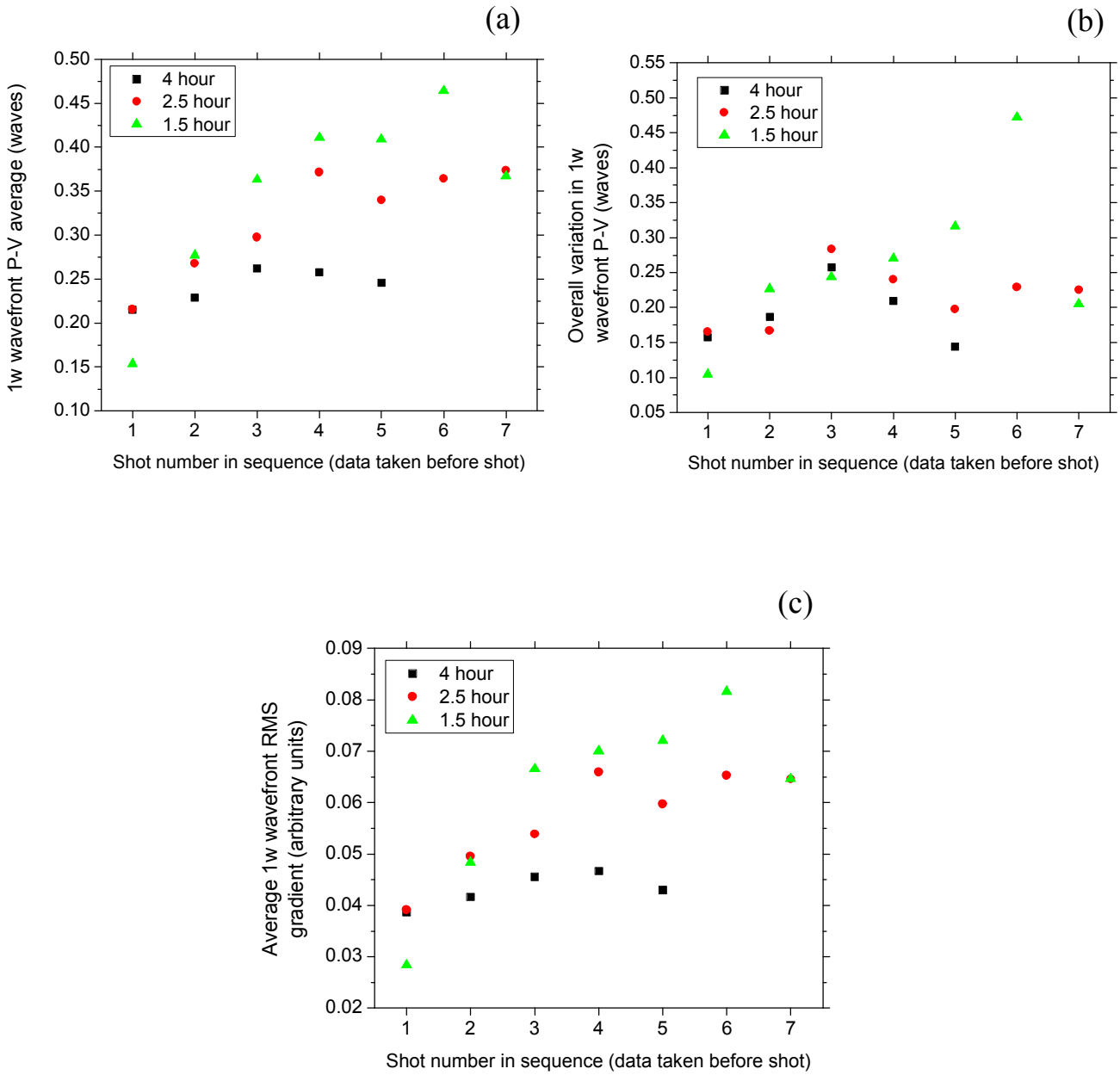

Fig. 12 - Wavefront distortion associated with convectively driven flows, as extracted from the PDS Hartmann sensor data. (a) The average wavefront P-V in each 40 image set. (b) The overall variation in the wavefront P-V in the 40 image set. (c) The average RMS gradient in each 40 image set (in arbitrary units).

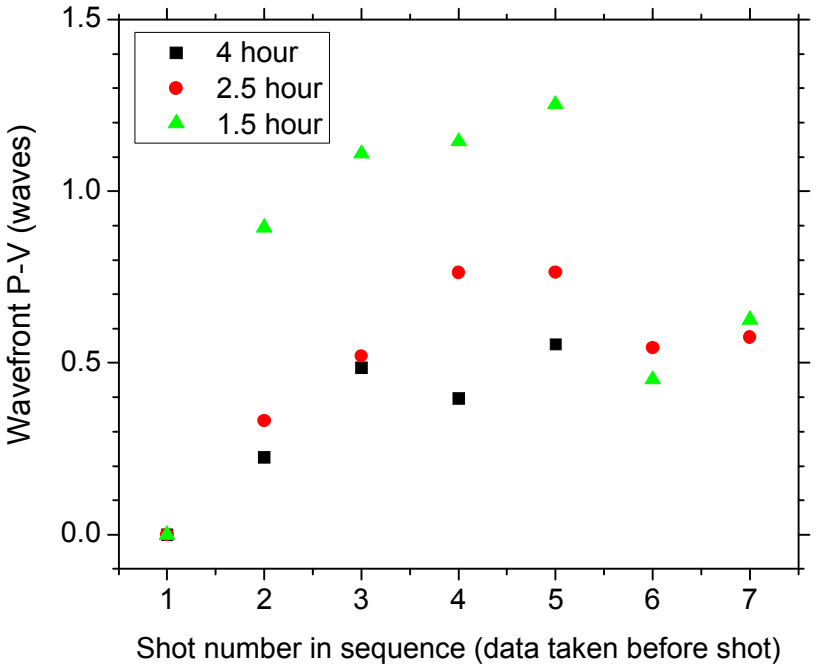

Fig. 13 - The quasi-static thermally induced wavefront distortion as extracted from the OSP Hartmann sensor data

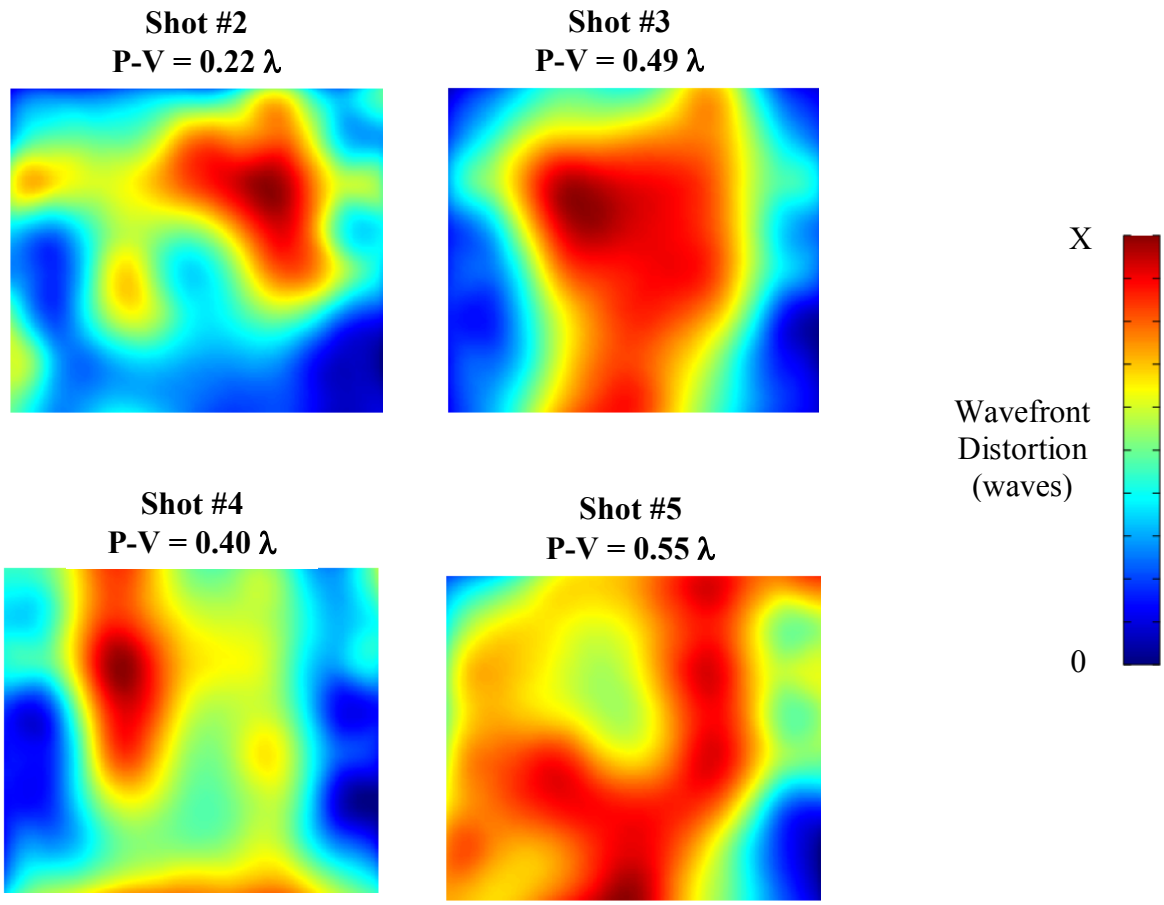

Fig. 14 - The spatial structure of the long time scale thermal distortion in the 4-hour shot period set. This data covers the inner 90% of the OSP Hartmann sensor beam footprint.

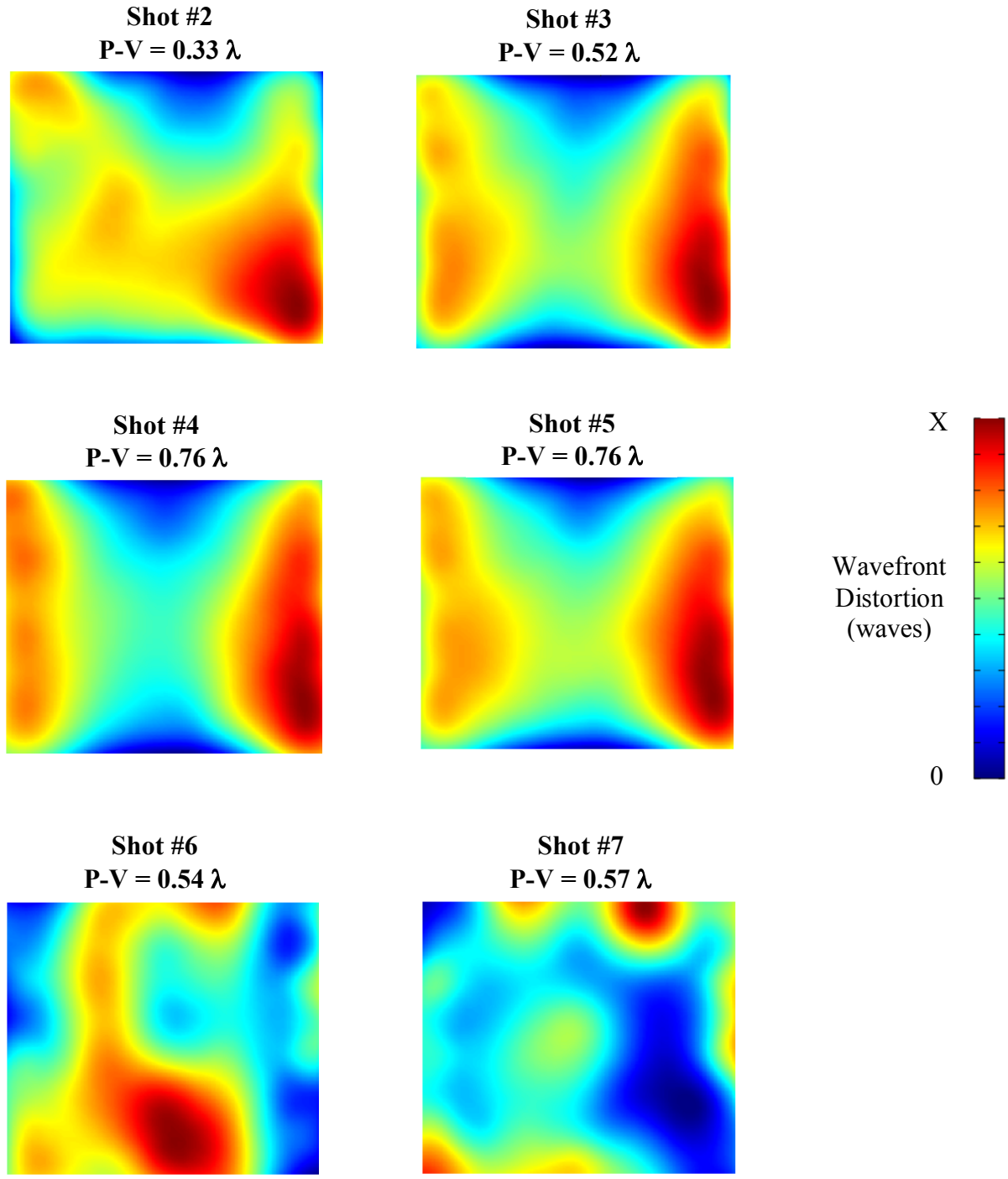

Fig. 15 - The spatial structure of the long time scale thermal distortion in the 2.5-hour shot period set. This data covers the inner 90% of the OSP Hartmann sensor beam footprint.

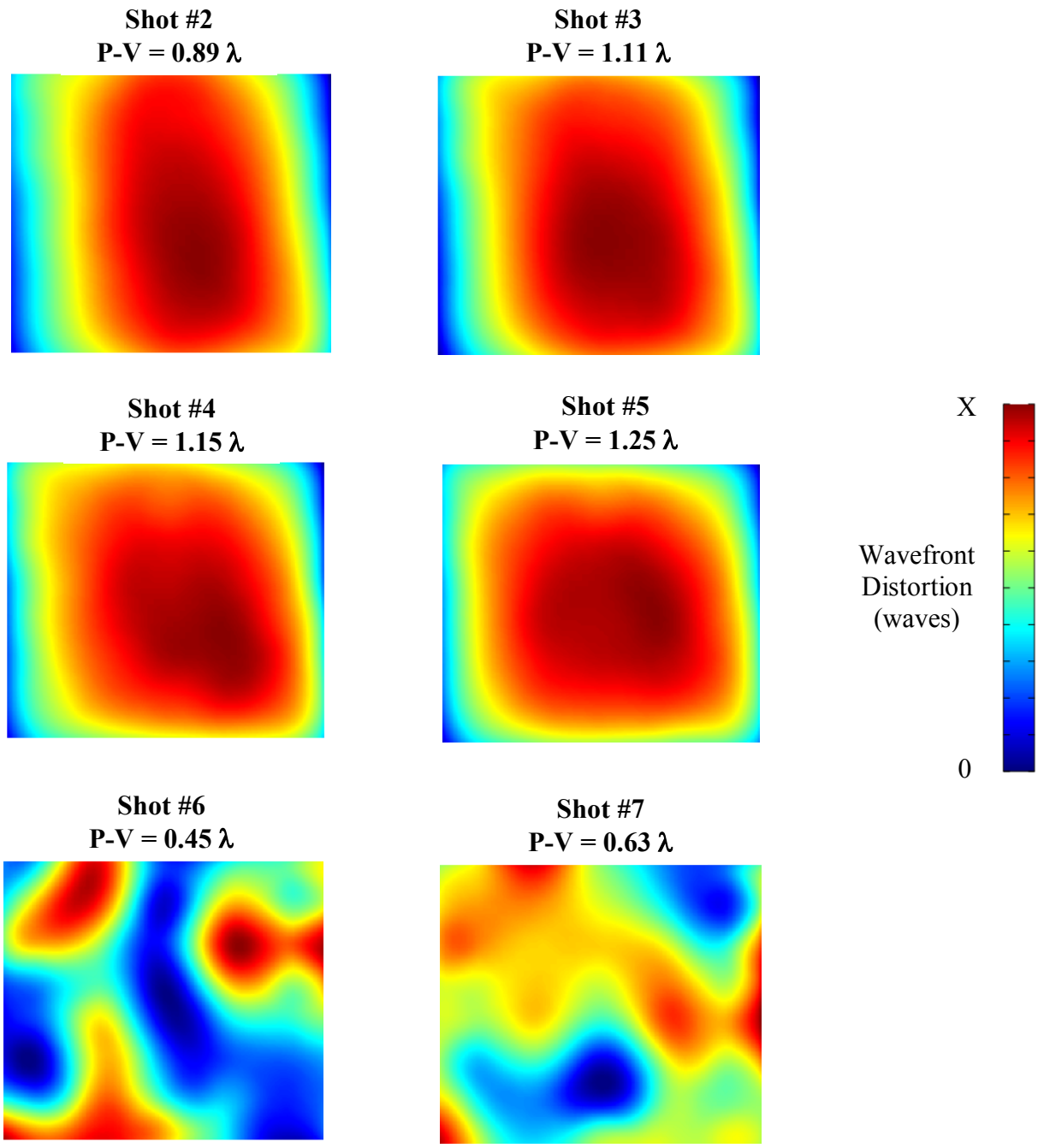

Fig. 16 - The spatial structure of the long time scale thermal distortion in the 1.5-hour shot period set. This data covers the inner 90% of the OSP Hartmann sensor beam footprint.

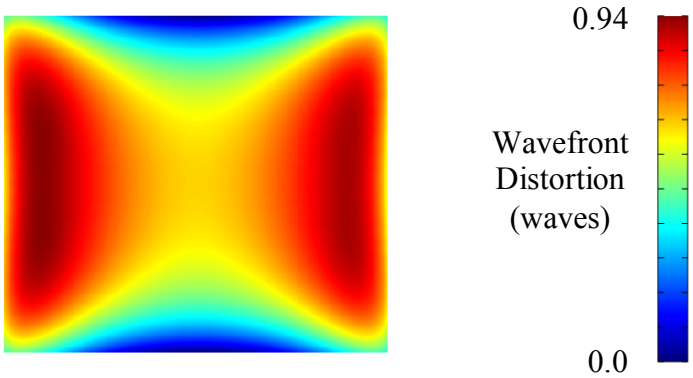

Fig. 17 - Model predicted system residual thermal optical distortion for an 11-7 configuration, 3 hours after a single flashlamp firing. This is based on simulation results provided by Wayne Miller.